

---

# TRAINING METHODS OF MULTI-LABEL PREDICTION CLASSIFIERS FOR HYPERSPECTRAL REMOTE SENSING IMAGES

---

A PREPRINT

**Salma Haidar \***

Department of Computer Science  
University of Antwerp, imec - IDLab  
Sint-Pietersvliet 7,2000, Belgium  
MicrotechniX BV

Anthonis de Jonghestraat 14 a, Sint Niklas,9100,Belgium

**José Oramas**

Department of Computer Science  
University of Antwerp, imec - IDLab  
Sint-Pietersvliet 7,2000, Belgium

January 18, 2023

## ABSTRACT

With their combined spectral depth and geometric resolution, hyperspectral remote sensing images embed a wealth of complex, non-linear information that challenges traditional computer vision techniques. Yet, deep learning methods known for their representation learning capabilities prove more suitable for handling such complexities. Unlike applications that focus on single-label, pixel-level classification methods for hyperspectral remote sensing images, we propose a multi-label, patch-level classification method based on a two-component deep-learning network. We use patches of reduced spatial dimension and a complete spectral depth extracted from the remote sensing images. Additionally, we investigate three training schemes for our network: *Iterative*, *Joint*, and *Cascade*. Experiments suggest that the *Joint* scheme is the best-performing scheme; however, its application requires an expensive search for the best weight combination of the loss constituents. The *Iterative* scheme enables the sharing of features between the two parts of the network at the early stages of training. It performs better on complex data with multi-labels. Further experiments showed that methods designed with different architectures performed well when trained on patches extracted and labeled according to our sampling method.

**Keywords** *Hyperspectral remote sensing images · computer vision · deep learning · multi-label classification · deep autoencoder · two-component networks*

## 1 Introduction

Hyperspectral imaging (HSI) technology combines the power of spectroscopy with digital optical imagery. It offers the potential to explore the physical and chemical composition of depicted objects that uniquely mark their behavior when interacting with a light source at different wavelengths of the electromagnetic spectrum. Historically, the technology was introduced in the remote sensing field [1]. However, it quickly spread to numerous other fields such as food quality and safety assessment, precision agriculture, medical diagnosis, artwork authentication, biotechnology, pharmaceuticals, defense, and home security [2], among others. Notwithstanding this richness of information, HSI does come with considerable challenges. Those are mostly related to the high dimensionality space due to the presence of numerous contiguous spectral bands, the large volume of data incompatible with the limited amount of the training data available, and the high computational cost associated. Such challenges render traditional computer vision algorithms insufficient to process and analyze such images [3]. The high dimensionality problem of hyperspectral images motivated several works. In general, two types of techniques were developed in this regard, in a supervised [4] or unsupervised learning manner. These are bands selection techniques [5, 6] which select the most informative subset of the bands, and feature extraction techniques [7] which transform the data to a lower dimension. In [8], a

---

\*Correspondent author, [salma.haidar@uantwerpen.be](mailto:salma.haidar@uantwerpen.be)

feature extraction method called improving distribution analysis (IDA) is proposed which aims to simplify the data and the computational complexity of the HSI classification model. [9] proposes a new semi-supervised feature reduction method to improve the discriminatory performance of the algorithms. Because finding a small number of bands that can represent the hyperspectral remote sensing images is difficult, [10] proposes a random projection algorithm applicable to large sized images that maintains class separability. Driven by this progress, hyperspectral image classification has received significant attention in the last decades leading to the development of high-performing methods. In [11], methods based on traditional machine learning and, more recent, deep learning techniques are proposed for hyperspectral image classification. Nevertheless, the need for large training data instances resulted in many of the deep learning-based methods to focus on the spectral aspect only. Yet, with the redundancy of information that contiguous bands cause, spatial features become essential to effect separability among the different classes. [12] exploits deep learning techniques for the HSI classification task proposing a method that utilizes both the spatial and spectral context to enhance the performance of the models. [13] presents a joint spatial-spectral HSI classification method based on different-scale two-stream convolutional network and a spatial enhancement strategy. [14] proposes an HSI reconstruction model based on deep CNN to enhance the spatial features. Graph Convolutional Networks (GCN) [15] have also been employed for hyperspectral image classification. [16] proposes a Multi-level Graph Learning Network (MGLN) for HSI classification. The current research mainly focuses on pixel-level, single-label classification and less on patch-level, multi-label classification. Therefore, unable to take advantage of the abundance of information that hyperspectral images contain. In this context, spectral unmixing [17] algorithms have been used to improve the HSI classification task by focusing on spectral variability. [18, 19] aim at identifying and separating the multiple spectra mix, called *endmembers*, present in one pixel. Our work adopts the deep learning approach in a supervised learning context. More specifically, we focus our analysis on breaking down the spatial stretch of the images into patches of smaller spatial dimension. We developed our model to preserve and explore the joint spatial-spectral characteristics by learning features that allow the identification of multiple objects in a reduced spatial surface. The model achieves this learning process using a deep autoencoder followed by a classifier. Moreover, considering that multiple objects/entities might occur within a depicted region, we formulate the prediction task as a multi-label prediction problem. Two-component classification networks exist in the literature; however, the formulation of the task of those networks focuses on specific terms concerning data and training. Data mainly refers to pixel-level, single-label data instances. When patches from the original images are used, those are densely sampled and assigned a single label corresponding to the patch's center pixel. to preserve the original size of the dataset. The training procedure of two-component networks mainly adopts the *Cascade* training as in [20]. Under the *Cascade* scheme, the feature extraction component of the network, i.e., the autoencoder is pre-trained separately. Next, the decoder is replaced by a classifier that is fine tuned to predict the correct label(s) while freezing the weights of the encoder. In addition, *Joint* training scheme also appears in the literature as in [21]; however, the focus of the study was mainly on analyzing the performance of the autoencoder in reconstructing inputs and less on the classification task. *Joint* training scheme refers to the process of training the two components simultaneously. In each epoch, the autoencoder trains to produce exact reconstructions from a compressed, hidden representation. At the same time, the classifier trains to predict the correct label(s) using the hidden representation as its input. In our work, we conducted a systematic analysis of different procedures, or *schemes*, that could be followed to train this two-component network. In this context, we identified three methods to train our network, the *Iterative*, the *Joint* and the *Cascade* training schemes.

The contributions of this paper are twofold. First, the hyperspectral image analysis focuses on patches with multi-labels to better represent the spatial-spectral aspect and the abundance of information of those images. This is in contrast to the single-pixel, single-label analysis commonly followed in the literature. We observe that the performance of a pixel-level, multi-class classifier drops when trained on patches with single labels corresponding to the center pixel. We conclude that the classifier will extract and learn more useful latent features embedded in the hyperspectral images when trained on the spatial-spectral extent available in those images combined with multi-labeled ground truth.

Second, we explore three training schemes in the multi-label prediction framework. Our results suggest that despite the superior performance of the *Joint* scheme, as shown by the results obtained, the *Iterative* scheme fostered early sharing of learnable features between the feature extraction component and the classifier resulting in improved performance and reduced overfitting. Moreover, we show that this scheme surpasses the commonly used *Cascade* training scheme and achieves improved performance on datasets characterized by an increased number of instances with multi-labeled ground truth.

This paper is organized as follows: Section 2 positions our efforts with respect to existing works in the literature. Section 3 presents the inner-workings of the proposed method, and the three training schemes considered in our analysis. Those are further validated in Section 4. Finally, we put forward concluding remarks in Section 5.

## 2 Related Work

Our analysis is related to the hyperspectral patch-level multi-label classification task employing deep models. We position our work based on closely related axes.

**Traditional machine learning as opposed to deep learning methods.** [22] summarizes the challenges of hyperspectral image classification that cannot be addressed by traditional machine learning. More specific to Remote Sensing, [23] provides an overview of the popular deep learning models to perform HSI classification. [24] provides a systematic review on the traditional neural networks and deep learning methods in environmental remote sensing applications, demonstrating that these methods have made tremendous progress in this field. All those papers focus their discussion and analysis on methods that perform pixel-level classification in a supervised manner, including deep belief networks, recurrent neural networks, and convolutional neural networks. In [25] the authors discuss the integration of traditional machine learning approaches with the deep learning techniques by investigating the application of Deep Support Vector Machines for HSI classification. All experiments performed reinforce the superiority of deep learning techniques over traditional machine learning. Our work follows this trend and focuses on learning representations from the data, automatically and hierarchically.

**Multi-label Prediction.** Compared to its single-label multi-class counterpart, multi-label prediction in HSI has received significantly less attention. [26] proposes a pixel-level, multi-label HSI classification method using a stacked denoised autoencoder (SDAE) combined with logistic regression. Results indicate that assigning multi-labels to a pixel can improve classification performance beyond the single-label approach. [27] proposes a multi-label classification algorithm based on the fusion of label-specific features. [28] investigates a feature extraction process to achieve multi-label classification for multi-spectral images. Even though no empirical evaluation on hyperspectral images is conducted, it emphasizes the importance of multi-label classification task for land cover in the context of spectral imagery. Our work adopts the same approach of multi-label predictions in the hyperspectral imagery domain. However, performing HSI classification using a group of pixels(patch) as input will only add to the complexity of the task since assigning one label to each patch will not be considered a realistic and satisfactory solution.

**Autoencoders as feature extraction method.** Autoencoders have been highlighted in several works [29, 30], as a successful representation learning method that improves the overall performance in HSI classification tasks. [31] utilizes a stacked denoised autoencoder (SDAE) for feature extraction followed by a logistic regression for fine tuning and classification. In [32], a spectral-spatial method is proposed which modifies the traditional autoencoder based on majorization minimization using multi-scale features. Finally, in [33] a methodology based on multi-view deep neural networks is proposed to fuse spectral and spatial features automatically extracted using two deep autoencoders. A semi-supervised graph CNN is then trained on these fused latent representations to perform HSI classification. Similarly, our work uses deep autoencoder as feature extraction method to learn relevant information from high dimensional data. In contrast to the works cited above, we use this information for multi-label classification.

**Patch-based Input data.** Patch-like input data instances whose spatial extent is smaller than the original hyperspectral remote sensing scenes have been used in the literature. However, unlike our work which annotates those patches with multi-labels, patches used in the literature were assigned single labels corresponding to the pixel located at the center of the patch. In this context, [34] proposes a convolutional neural network for hyperspectral image data. Spectral-spatial features are extracted from the original scene, starting from a target pixel and densely sampling neighboring pixels in the form of  $n \times n \times bands$ . Next, a single label corresponding to the central pixel of that neighbourhood/patch is assigned. The sampling process adopted preserves the number of labeled pixels available in the original remote sensing scene. Several one-dimensional feature vectors are obtained using a 3-dimensional convolutional layer. Next, the vectors are reshaped into two-dimensional image matrix and fed into a standard CNN.

## 3 Proposed Method

In this section, we present the proposed model to perform the patch-based multi-label classification. Figure 1 illustrates the model architecture and data flow route. It is composed of two main components, an autoencoder and a classifier. Patches of reduced spatial and full spectral dimensions are sampled from the original remote sensing scene and passed into the network. While the autoencoder reduces the dimensionality and preserves the essential features of the data to perform the reconstruction task, the classifier will highlight the discriminatory aspects in the hidden representation of the autoencoder to identify different classes (multi-labels) present in one patch.

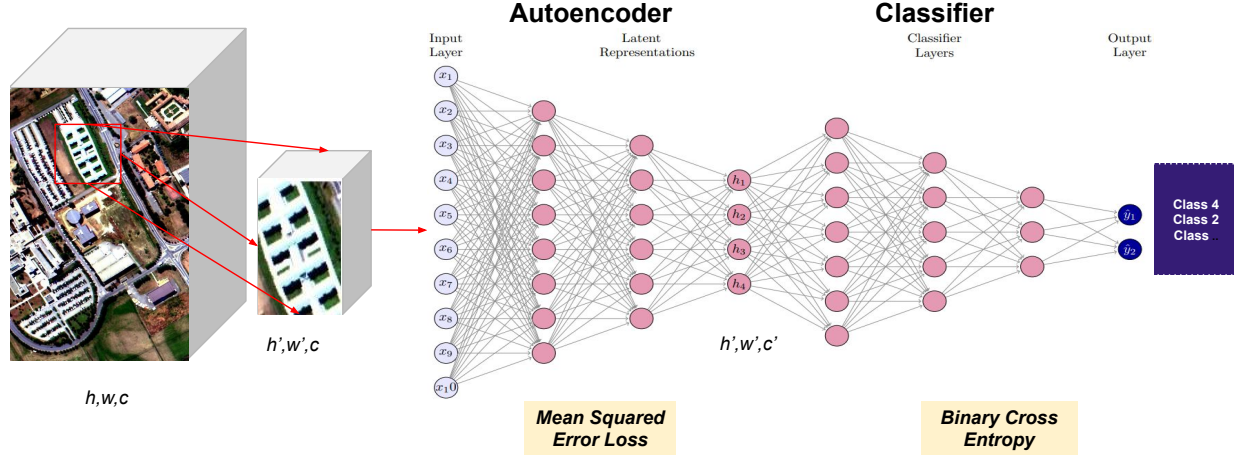


Figure 1: Two-components hyperspectral image classification network composed of a deep autoencoder that feeds its hidden representation into a classifier.

### 3.1 Model Architecture and description

**Input data** Our input data is of size  $X \in \mathbb{R}^{h,w,c}$ ,  $h, w$ , and  $c$  being the height, width, and the number of spectral bands, respectively. We start from a full scene and sample small patches of size  $p \in \mathbb{R}^{h' \times w' \times c}$ .  $h', w', c$ , being the height, the width, and the spectral bands of the patch, respectively. We do that by chopping the original scene using a window of size  $(3, 3)$  and applying a stride of 3 to prevent overlapping of our patches. Next, we assign multiple labels to those patches, representing the classes in each patch. For further processing, we encode our multi-labels into one hot encoded vector where 1 indicates the presence of the classes associated with each patch.

**Autoencoder.** The autoencoder extracts features that will preserve essential information embedded in the spatial-spectral dimension of the input data.

The first group of layers, the encoder, receives the patches, processes them, and passes them to the subsequent layers. It then gives its output to the decoder and the second component of the network. The autoencoder's hidden layer or hidden representation represents the encoder's output. It is a compressed version of the input data encoded in the form of a vector of size  $h \in \mathbb{R}^{h' \times w' \times c'}$ ,  $c'$  being the reduced number of the spectral bands. The decoder group of layers deconvolves the compressed data into a fully reconstructed input instance.

Table 1: Autoencoder: Layers' Architecture

Layer	Input Shape	Output Shape
<b>Encoder:</b>		
Linear⇒dropout⇒relu	[1, 3, 3, bands]	[1, 3, 3, 96]
Linear⇒dropout⇒relu	[1, 3, 3, 96]	[1, 3, 3, 64]
Linear⇒relu	[1, 3, 3, 64]	[1, 3, 3, 32]
<b>Decoder:</b>		
Linear⇒dropout⇒relu	[1, 3, 3, 32]	[1, 3, 3, 64]
Linear⇒dropout⇒relu	[1, 3, 3, 64]	[1, 3, 3, 96]
Linear	[1, 3, 3, 96]	[1, 3, 3, bands]

In addition to dimensionality reduction, the autoencoder reduces redundant information by eliminating redundant neighboring spectral bands. Those bands do not offer any additional discriminatory information yet they contribute to the high volume/dimension of the hyperspectral data.

Equations 1 and 2 provide a mathematical representation of the inner workings of the autoencoder layers.

$$h = f(W_h \times x + b_h) \quad (1)$$

$$y = g(W_y \times h + b_y) \quad (2)$$

$W_h$  and  $W_y$  stand for the weights of the encoder and the decoder layers respectively.  $b_h, b_y$ , in turn, resemble the bias of both layers.  $f$  and  $g$  are the Rectified Linear Unit (ReLU) activation function used to perform element-wise non-linear transformation for the autoencoder. Once the input has been reconstructed we measure the reconstruction error. Towards that end our objective function is the Mean Squared Error (MSE). By minimizing this loss, the reconstruction capability of the autoencoder will be optimized.

**Classifier.** The multi-label prediction classifier will learn a function that maps an instance  $x' = \{x'_1, x'_2, \dots, x'_n\} \in X'$ , to a subset  $l \in \mathbb{R}^c$  where  $c$  represents the entire classes in the labeled dataset. The space of labels accordingly is  $y = \{0, 1\}^c$ . Worth noting that  $X' \in \mathbb{R}^{h' \times w' \times c'}$  represents the set of hidden representations generated by the autoencoder component of our model.

Four fully connected layers define the architecture of the classifier. Patches are passed through the encoder, in batches, to output a compressed version of each patch. The compressed patches will be flattened to size  $X' \in \mathbb{R}^{h' \times w' \times c'}$ , before being passed on to the classifier to predict the label(s) of classes occurring in the input patch. We used the ReLU activation function and passed a dropout regularization method in each sequential layer during training.

Table 2: Classifier: Layers' Architecture

Layer	Input	Output
<b>Classifier:</b>		
Linear⇒dropout⇒relu	[1, 288]	[1,3000]
Linear⇒dropout⇒relu	[1, 3000]	[1,1512]
Linear⇒dropout⇒relu	[1,1512]	[1,512]
Linear⇒dropout⇒relu	[1,512]	[1,28]
Linear⇒relu	[1,28]	[1,classes]

The output layer will generate logits. Predictions  $\hat{y}$  are made by applying sigmoid function to the output logits. In Equation 3, values  $> 0.5$  will indicate the presence of the corresponding labels at that position.

$$\hat{y} = [\hat{y}_{ci} > 0.5] \text{ where } i \in \{1, \dots, N\} \quad (3)$$

We optimize the performance of the classifier by training a Binary Cross Entropy with Logits Loss as the objective function of the model (equation 4). This function combines the Binary Cross Entropy (BCE) loss used for binary classification with a Sigmoid activation,  $\sigma(x) = \frac{1}{1+e^{-x}}$  instead of a Softmax activation  $\sigma(x_i) = \frac{e^{x_i}}{\sum_{j=1}^c e^{x_j}}$  for  $i = 1, 2, \dots, c$ . BCE with Sigmoid produces a probability score for each label. The calculated loss is independent for each label meaning that the loss computed for one label is not impacted by the loss calculated for another label. This is logical because in multi-label classification classes are not mutually exclusive.

$$l_{n,c} = -w_{n,c} [p_c y_{n,c} \times \log \sigma(x_{n,c}) + (1 - y_{n,c}) \times \log(1 - \sigma(x_{n,c}))] \quad (4)$$

where  $c$  is the class number,  $n$  is the number of the sample in the batch and  $p_c$  is the weight of the positive answer for the class  $c$ .

Tables 1 and 2 illustrate the layers of each network component providing details concerning the shapes of the input and output of each layer. The last layer of the classifier will output the predictions, considering the number of classes in each dataset and the conducted experiment. Given the structure of our experiments, we did not ignore the background class in our multi-label predictions. However, the background class was ignored entirely in experiments related to single-label prediction. The shape of the output layer will change according to each experiment by including or excluding the background class found in each dataset when necessary.

### 3.2 Training and validation process

In architectures featuring two-component networks, the training process usually occurs in one of two distinct schemes: *Joint* and *Cascade*. This paper analyzes a third scheme, the *Iterative* training scheme. While ensuring progressive and separate training of both components, this scheme allows early sharing of features. *Iterative scheme*. Under this scheme, the autoencoder and the classifier are two separate architectures, each with a different objective function. Training is performed in iterations of a predefined number of epochs and alternated between both architectures. We initialize the autoencoder, allow it to train for a set of epochs, and save it. Next, we initialize the classifier, load the

saved autoencoder and pass the partially trained encoder to the classifier. To this end, our model consists of an encoder and a classifier, and the encoder’s parameters are frozen to prevent retraining. Meanwhile, we allow the classifier to train for a set of epochs. This operation is repeated throughout the complete training process of the network. Even though one model is idle while the other is training, having the partially trained encoder together with the classifier at every training iteration exerts a direct impact on the performance of the classifier. At a very early stage, the classifier will learn some features that the autoencoder deemed informative for reconstruction. These features are also helpful for the prediction task.

*Joint scheme.* Under this scheme, the two components form one algorithm. Data is passed and processed in sequence from the first component (the autoencoder) to the following component (the classifier), which will perform the prediction. Input data is routed into the autoencoder that generates two outputs, (1) a reconstruction of the input and (2) a hidden, compressed representation fed into the classifier’s layers to predict a multi-label output. The loss objective in this scheme is a weighted combination of the autoencoder’s and the classifier’s loss objectives. In our experiment, the total loss combination consists of 30% weight of the classifier loss and 100% of the autoencoder loss. We experimented with several pairs of weights until we reached this combination that generated a good performance. In the backpropagation pass, all losses train simultaneously—the autoencoder trains to produce better reconstructions, and the classifier trains to improve its predictions. Total loss, a predefined weighted combination, generates a form of normalized loss.

*Cascade scheme.* Under this scheme, the feature extraction component is trained separately to perform the reconstruction of the input and trained weights are saved. The pre-trained model is loaded in the following step, and the encoder layer is passed into the classifier. Weights of the pre-trained encoder are frozen, allowing only the classifier to train. This is in contrast to the *Iterative* scheme, where the classifier’s training occurs progressively following a progressive, partial training of the autoencoder. In *Cascade* training, with every training epoch, one forward pass and one backward pass are completed. In the backward propagation call, however, only the gradients of the classifier weights are calculated since all weights of the encoder layer are frozen.

### 3.3 Implementation details

We trained, validated, and tested a multi-label prediction model on hyperspectral images of low spatial dimension. These images have a height and width of 3 pixels, respectively, and a depth equivalent to the number of bands of the entire original scene they were sampled from. Height and width lower than  $3 \times 3$  produced many patches with only one class. The larger size resulted in a reduced number of patches. We normalized the values of our data by applying z-score normalization such that our data’s mean and standard deviation are approximately 0 and 1, respectively. We applied the Adam optimization algorithm [35].

Depending on the experiment conducted, we also selected and tuned a set of hyperparameters, such as learning rate, batch size, and drop-out rate, for training the autoencoder and the classifier. The learning rate in this context ranged from  $1e^{-5}$  to  $1e^{-2}$ , and the batch size ranged between 100 to 240.

Common to both the autoencoder and the classifier is the application of the learning rate scheduler, a mechanism applied during the training process that supports faster conversion. Learning rates gradually reduce at a step size corresponding to a predefined number of epochs at a multiplicative factor of the learning rate denoted by  $\gamma = 0.9$ . Full details on the different hyperparameters applied under various training schemes can be found in the supplementary material to this paper. Furthermore, training the network produces several trainable parameters. In general these range from 35,615 to 56,108 trainable parameters for the autoencoder, and from 6,193,822 to 6,194,025 trainable parameters for the classifier. The observed differences result from modifications introduced into the model to reflect the intrinsic aspects present in the data. In particular, the number of classes differs between the two datasets used in our experiments. On the one hand, PaviaU has 10 classes including the background class. On the other hand, Salinas has 17 classes, including the background class. Moreover, the number of bands differs between the two sets; 103 for PaviaU and 204 for Salinas.

### 3.4 Datasets

Our method was evaluated on two publicly available datasets of remote sensing scenes [36], (Figure 2). **Pavia University Scene** (PaviaU), a hyperspectral scene acquired by the ROSIS sensor over the University of Pavia in Italy. It has 103 spectral bands ranging from  $0.430 \mu\text{m}$  to  $0.86 \mu\text{m}$  in wavelength, a spatial size of  $610 \times 340$  pixels and a geometric resolution of 1.3 m. The ground truth consists of 9 different classes including trees, asphalt, meadows, among others in addition to undefined class labeled background. Only 20.6% of the pixels have labels corresponding to the 9 classes, the rest are labeled as background. **Salinas Scene**, a hyperspectral scene collected by the AVIRIS sensor over Salinas Valley, California. It has a spatial size of  $512 \times 217$  pixels and a spatial resolution of 3.7 m. The original scene

had 224 spectral bands ranging from  $0.4\text{ }\mu\text{m}$  to  $2.5\text{ }\mu\text{m}$  in wavelength but 20 water absorption spectral bands have been discarded. The ground truth contains 16 classes including vegetables and vineyard fields among others in addition to undefined class, labeled background. Only 40.8% of the pixels have labels corresponding to the 16 classes, the rest are labeled as background.

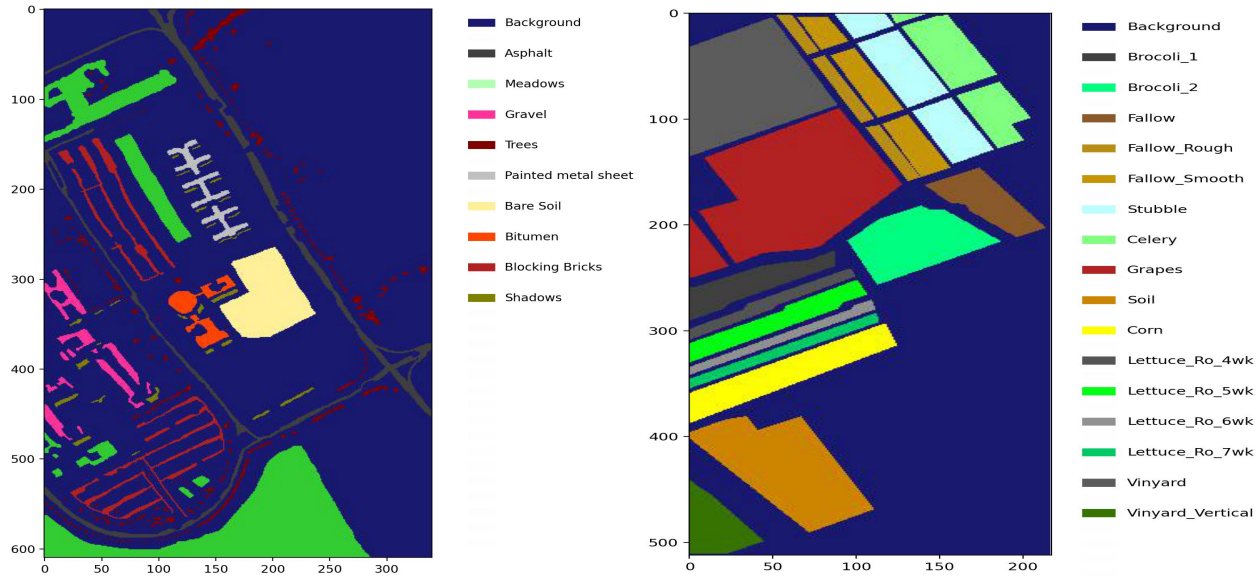


Figure 2: Hyperspectral Remote Sensing Scenes. *Left*: Pavia University Scene, *right*: Salinas Scene

**Patch creation and label assignment.** We transformed the scenes, from the aforementioned datasets, by performing a slicing operation across the columns and rows. We have done that without allowing any overlapping and while preserving the original depth of the scene, i.e. the number of spectral bands. The result is low spatial dimension patches of size  $(3, 3, \text{bands})$ . Next we adopted two different approaches to assign labels to patches. First, *Multi-label sampling* where labels were assigned to the patches extracted based on the classes present in the patch. Patches made up fully of pixels with undefined class (background) were completely ignored. However, if the background class exits in a patch together with other classes the patch is kept and the label would include the background class. The resulting data contained a mix of both patches with multi-labels and patches with only single labels indicating that the patch is uniform, consisting of pixels belonging to the same class. Second, *Single-label sampling* where patches were assigned labels corresponding to the center pixel of the patch regardless of the classes of surrounding pixels. Patches where the center pixel represented the background class, were ignored. The resulting data is fully single labeled however the patches themselves were made of two different pixel distributions. On the one hand, there are the uniform patches whose pixels belong to the same class and represent approximately 64% and 88% of PaviaU and Salinas respectively. On the other hand, there are the mixed patches whose pixels belong to different classes including the background but the center pixel is never a background class. Those represented 36% and 14% of PaviaU and Salinas respectively. Table 3 illustrates the resulting patches and labels count.

Table 3: Patches sampled from PaviaU and Salinas datasets using Multi-label and Single-label sampling procedures

	<i>PaviaU</i>	%	<i>Salinas</i>	%
<b>Multi-Label Sampling</b>				
<i>multi-labels mixed</i>	3774	55%	1442	21%
<i>single-labels uniform</i>	3125	45%	5289	79%
<b>Total</b>	6889	100%	6731	100%
<b>Single-Label Sampling</b>				
<i>single-labels mixed</i>	1742	36%	721	12%
<i>single-labels uniform</i>	3097	64%	5290	88%
<b>Total</b>	4839	100%	6011	100%

Finally, we split the data under both approaches into train, valid and test sets adhering to approximately 80%, 10%, 10% ratios respectively, (Table 4). The data, model architecture and code used in our experiments will be publicly released upon acceptance of this submission.

Table 4: Train, Valid and Test split of patches dataset

	<i>Multi-label Patches</i>			<i>Single label Patches</i>		
	<i>Train</i>	<i>Valid</i>	<i>Test</i>	<i>Train</i>	<i>Valid</i>	<i>Test</i>
<i>PaviaU</i>	5588	621	690	3919	436	484
<i>Salinas</i>	5451	606	674	4868	541	602

## 4 Results and Discussion

### 4.1 Multi-Label Classification: Performance Across Training Schemes

This experiment compares the results of the three schemes presented in Section 3.2 in the context of the task at hand, i.e., multi-label classification on hyperspectral patch images. Under each scheme, we adopted the same architecture for the autoencoder and the classifier regarding the number of layers and input dimension. However, we applied different hyperparameters per scheme and dataset used. Those hyperparameters were tuned to achieve the optimal performance under each setting. We apply weight regularization L2-norm to the classifier loss in all three schemes. Accordingly, the loss function of the classifier, Equation 4, became a new loss function after adding the regularization term.

$$l_{n,c} = -w_{n,c}[p_c y_{c,n} \times \log \sigma(x_{n,c}) + (1 - y_{n,c}) \times \log(1 - \sigma(x_{n,c}))] + \lambda \sum_{i=1}^n ||w_i^2|| \quad (5)$$

where  $\lambda$  represents a hyperparameter that scales the level of penalty introduced by the regularization to reduce the weights of the parameters, rendering the model simpler and less prone to overfitting. Since our task is that of multi-label classification, we adopted the standard multi-label evaluation metrics as in [37]. More specifically, the *Accuracy*, the *Hamming Loss*, the *Precision*, and the *Recall*. Please refer to the supplementary material for the equations related to these metrics. According to [37], in the context of multi-label classification, the accuracy metric accounts for partial correctness, whereby the accuracy for each instance is the proportion of the predicted correct labels to the total number (predicted and actual) of labels for that instance. Overall accuracy is the average across all instances. Since we also experiment with single-label, multi-class classification, we focused our attention on *Accuracy* to perform a comparison among the different experiments we conducted.

Table 5: Multi-label Classifier: performance evaluated on multi-label patches test dataset sampled from PaviaU

	<i>Iterative</i>	<i>Joint</i>	<i>Cascade</i>
<b><i>Accuracy</i></b>	84.03%	86.14%	83.5%
<b><i>Hamming Loss</i></b>	0.037	0.3	0.04
<b><i>Precision</i></b>	0.88	0.91	0.87
<b><i>Recall</i></b>	0.89	0.93	0.87

Table 6: Multi-label Classifier: performance evaluated on multi-label patches test dataset sampled from Salinas

	<i>Iterative</i>	<i>Joint</i>	<i>Cascade</i>
<b><i>Accuracy</i></b>	87.61%	86.40%	86.47%
<b><i>Hamming Loss</i></b>	0.015	0.017	0.02
<b><i>Precision</i></b>	0.89	0.89	0.88
<b><i>Recall</i></b>	0.93	0.90	0.92

**Results:** Tables 5 and 6 present an overview of the results achieved by each scheme based on the test split of the PaviaU and Salinas patches datasets. We observe that the *Cascade* scheme underperformed the other two schemes even with the Salinas dataset, which contains a significant number of uniform patches. Considering that the *Cascade* scheme is one of the commonly followed training schemes in the literature, [31] and, [20], this comes as a surprise. Moreover, *Joint* training outperformed the other two schemes in making predictions of multiple labels, mainly when tested on the PaviaU dataset. Comparing results between the two datasets, we recognize that all three schemes performed better under PaviaU in making predictions of multiple labels than under Salinas. Worth noting that the PaviaU patches dataset contains double as many instances with multiple labels as Salinas, (Table 3).



## 4.2 Effect of Ground-Truth Annotations on Performance

We conducted this experiment to investigate the observations made in Section 4.1. We divided the results achieved under the mentioned experiment according to the number of ground-truth labels assigned to each patch in the test dataset. In this context, *multi* refers to those patches sampled under the *multi-label sampling* approach (Section 3.4) whose outcome is an annotation containing several labels reflecting the classes found in the patch. *Single*, refers to patches sampled under the same approach. However, the resulting patches contain pixels belonging to one class only. In this sense, the annotation would be a single label. In this experiment, we mainly focus on classification accuracy as a performance metric, and we base our results on the patches test datasets sampled from PaviaU and Salinas, respectively.

Table 7: Multi-label Calssifeir: model accuracy performance based on multi-label and single-label patches

	<i>Iterative</i>		<i>Joint</i>		<i>Cascade</i>	
	<i>multi</i>	<i>single</i>	<i>multi</i>	<i>single</i>	<i>multi</i>	<i>single</i>
<i>PaviaU</i>	84.75%	83.03%	86.29%	85.74%	84.31%	83.16%
<i>Salinas</i>	70.61%	92.40%	74.55%	89.73%	67.79%	91.73%

**Results:** Table 7 presents a breakdown of the accuracy by the type of label. In conformity with the conclusion drawn in the previous experiment, all schemes had higher accuracy in predicting multi-label patches when such patches are dominantly present in the dataset, as is the case with the PaviaU dataset. Additionally, within the same multi-label context, the *Joint* scheme remained the highest performing scheme.

The performance reverses when patches containing only one class are dominant, as with patches sampled from Salinas. All three schemes performed better when considering Salinas dataset and the single-label patches. This experiment shows that the larger the number of multi-labeled patches, the higher the *Iterative* and *Joint* schemes’ accuracy in predicting those multi-labels compared to that of the *Cascade* training scheme.

Furthermore, when examining the training and validation loss patterns, Figure 3, we find that the *Iterative* scheme converges slower to lower loss values. Nevertheless, it does not expose the model to overfitting, as is the case with the *Cascade* scheme. Even though the loss function optimized under the *Joint* training scheme is not directly comparable to the loss function optimized for the *Iterative* scheme, the former depicted a better behavior when it comes to a faster convergence and lower loss values.

It is worth indicating, though, that the total loss of the *Joint* scheme contains only 30% of the stand-alone classifier loss. We can also see the impact of such contribution on the average accuracy performance of the *Joint* training in Figure 4. We observe broad and dense oscillations. Those oscillations indicate that the autoencoder has not learned the features that can help the classifier make a correct decision consistently. Examining the classifier loss component separately, we notice that it exhibits a more significant overfitting trend whose impact is diluted in the overall loss due to the low contribution of the classifier loss. If we choose another pair of weights, performance will also change, not necessarily for the better. This renders the process sensible to changes caused by other hyperparameters.

## 4.3 Single-Label Classification: Performance Across Training Schemes

This experiment examines the classification performance of our network under the three training schemes using single labeled patches. We sampled those patches under the single-label sampling approach described in Section 3.4. To this end, we implemented several changes to adapt the three schemes to the new type of labels.

First, we adjusted the output layer of the classifier to reflect the number of classes after ignoring the background class. Second, we tuned a new set of hyperparameters for each method and under each dataset. Third, we adjusted the loss function to fit the new task of single-label multi-class classification. For such a task, the Cross-Entropy Loss Function applies, (Equation 6).

$$l = - \sum_{c=1}^C y_{n,c} \log(p_{n,c}) \quad (6)$$

Where  $n$  is the input,  $y$  is the target,  $c$  is the number of classes. Finally, for evaluation, we adopted the single-label multi-class accuracy metric calculated as the proportion of all correct predictions to the total number of data instances tested.

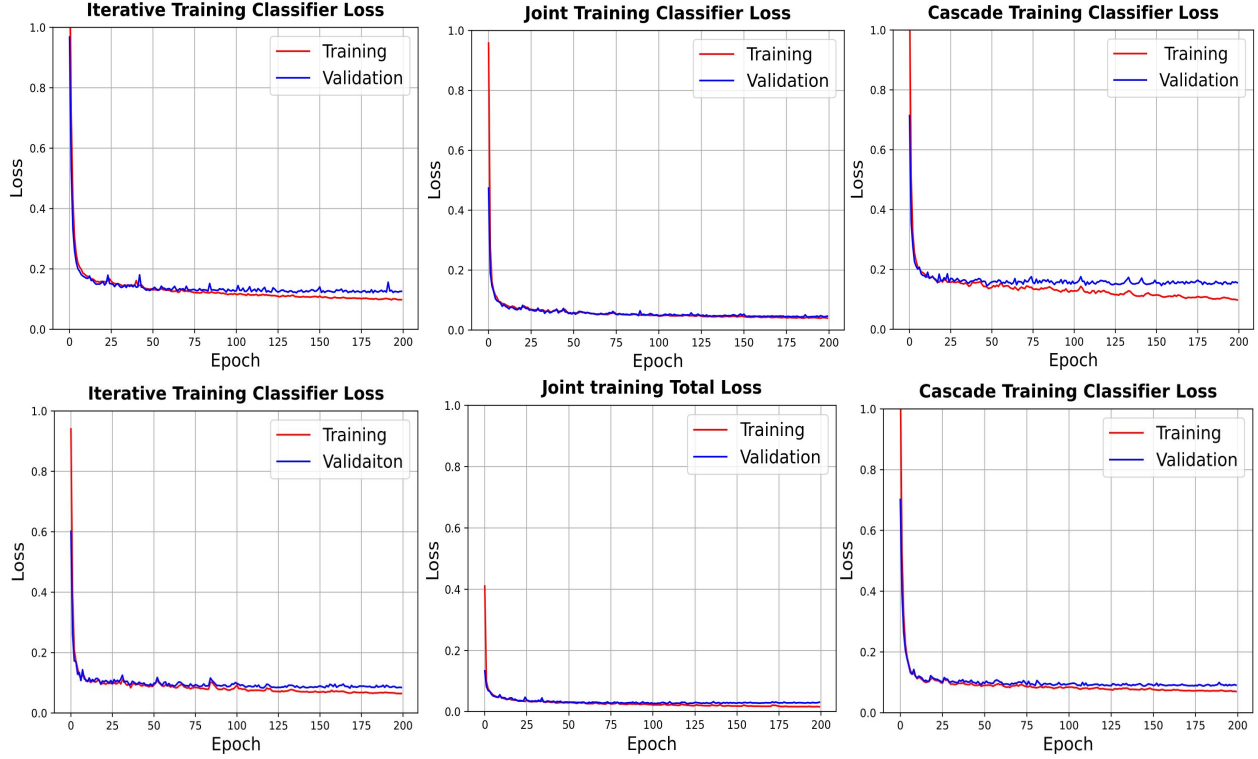


Figure 3: Multi-label Classifier: Train and valid loss under the three schemes. Above: PaviaU, Below: Salinas

Under this experiment, we also applied the weight regularization L2-norm to the classifier loss in all three schemes. Accordingly, the loss function of the classifier, as shown in Equation 7 became a new loss function.

$$l = - \sum_{c=1}^C y_{o,c} \log(p_{o,c}) + \lambda \sum_{i=1}^n ||w_i^2|| \quad (7)$$

Table 8: Single-label Classifier: performance evaluated on single-label patches test datasets sampled from PaviaU and Salinas

	<i>Iterative</i>	<i>Joint</i>	<i>Cascade</i>
<i>PaviaU</i>	90.71%	94.65%	87.73%
<i>Salinas</i>	91.19%	93.35%	90.34%

**Results:** Table 8 presents the accuracy obtained across the different schemes per each dataset. The *Joint* scheme achieved the highest accuracy of 94.65% and 93.35% on the testing sets from PaviaU and Salinas, respectively. It was followed by the *Iterative* scheme on both datasets. Similar to the multi-label classification task, the *Cascade* scheme came third with 87.73% and 90.34%, respectively.

Figures 5 and 6 illustrate the loss and accuracy performance of each scheme on both the PaviaU and Salinas datasets. Combined with the results presented in Table 8 and despite the overall generalization of the three schemes, the *Iterative* and *Joint* schemes exhibited overfitting and stagnation during the learning process. Additionally, this performance was obtained faster and in the earliest epochs for the *Joint* training scheme. The total loss optimization under the *Joint* training scheme contributes to the divergence of the validation loss. Since the total loss is a weighted combination of the network’s two-components loss functions, with a higher influence given to the autoencoder, the performance of the classifier dropped at validation. This reduced performance indicates that features compressed in the hidden layer of the autoencoder were probably not the essential features representations useful for the classifier. The *Cascade* scheme, by contrast, converged better than the rest yet, it required a much lower learning rate  $1e^{-5}$ , justifying the convergence of loss and rise in accuracy only towards the last 50 epochs of the training.

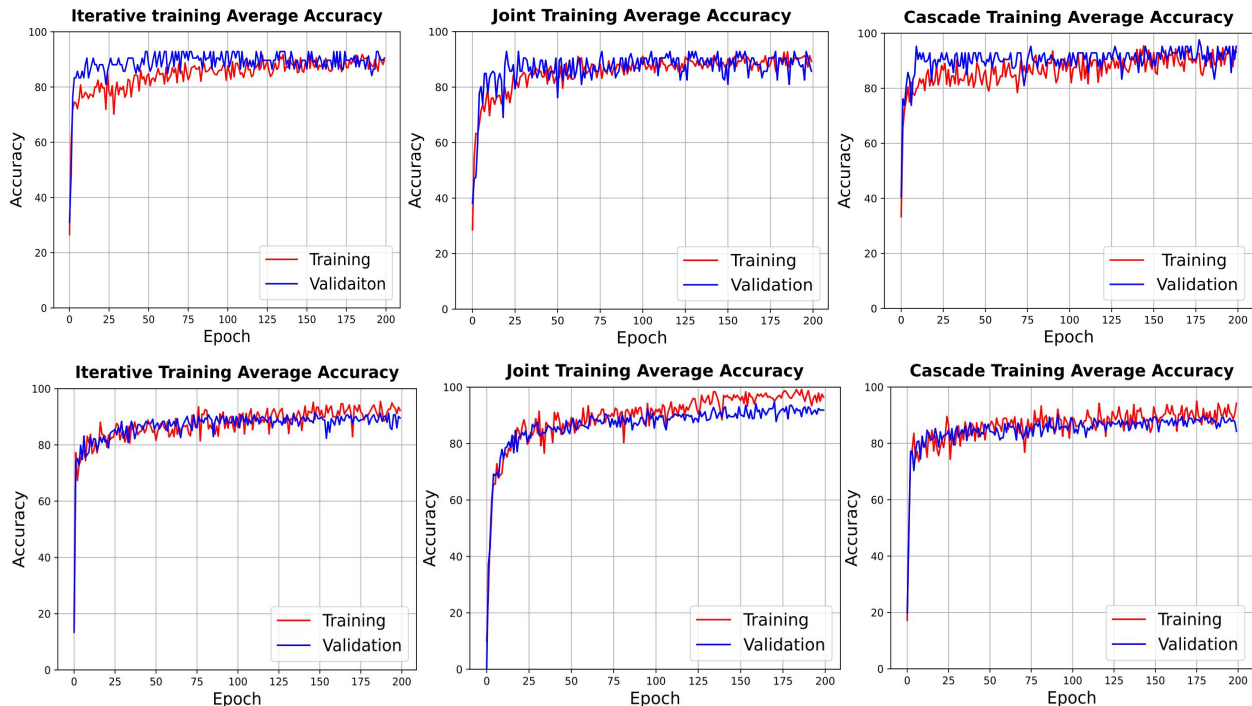


Figure 4: Multi-label Classifier: average accuracy performance. *Above*: PaviaU, *below*: Salinas

Furthermore, the *Iterative* scheme exhibited a similar behavior as the *Joint* scheme in terms of divergence of the validation loss. However, since the architecture of the *Iterative* scheme permits indirect interaction between the learned weights of the autoencoder and the classifier early on, we observe that the divergence between the training and validation loss does not occur immediately and it maintains a flat level going further.

For the case of the Salinas dataset, a higher percentage of the sampled patches are uniform patches consisting of one class only. Labels, however, correspond to the center pixel of the patch. We notice in Figures 5 and 6 that again smoothed by the weighted sum of the loss functions of the individual components (the mean squared error and the binary cross entropy), the *Joint* scheme total loss creates a smooth convergence to a low loss level. Based on the accuracy achieved employing the *Joint* scheme on the validation set, it appears that the single label classifier was stable and consistent in capturing the learned features when making its decision at every epoch. This contrasts with the performance of the same scheme on PaviaU and within the multi-label experiment (Figure 4). Moreover, when making its predictions, the classifier trained by the *Iterative* scheme shows a consistent learning process as reflected by the minimal oscillations of the accuracy curves in Figure 6. We link that primarily to the complex progressive nature of learning between the two parts of the network. Because uniform patches are dominant in the Salinas patches dataset, the learning process of the feature representations by the classifier seems to be easier than in the case of PaviaU.

#### 4.4 Single-label Classification: Impact of Domain Shift on Performance

To further examine the performance of the single-label classifier, we tested the classifier that was trained in Section 4.3 on two new subsets of PaviaU and Salinas. We assembled those subsets from the patches generated under the *Multi-label sampling* approach (Section 3.4) that are uniform, i.e. containing only one class as opposed to patches containing mixed classes. Consequently, we assigned the single labels of those patches based on the classes occurring in the patch and not based on the class corresponding to the center pixel. Worth noting that the center pixel procedure for the label assignment characterizes the data that initially trained our single-label classifier. Therefore, this experiment aims at assessing the effect of this disparity arising from training the single classifier on a combination of mixed and uniform patches, yet testing it on only uniform patches.

**Results:** Table 9 summaries the results. At first sight, the drop in performance is noticeable compared to the results reported in Table 8. For the case of the PaviaU dataset, we notice a drop of 12.31%, 2.42% and 9.56% across the *Iterative*, *Joint* and *Cascade* schemes, respectively. For the Salinas dataset, we notice an improvement in the

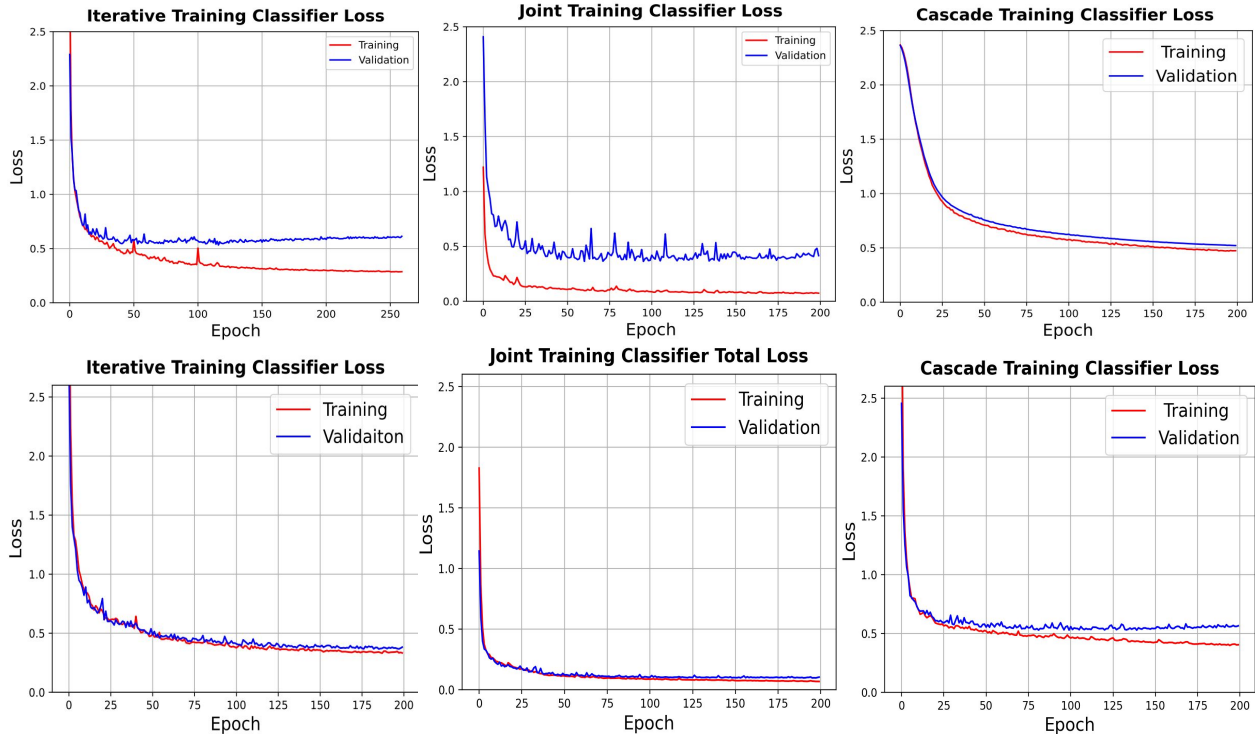

 Figure 5: Single-label Classifier: train and valid loss of the three methods. *Above: PaviaU, below: Salinas*

Table 9: Single-label Classifier: performance on uniform single-label patches

	<i>Iterative</i>	<i>Joint</i>	<i>Cascade</i>
<i>PaviaU</i>	78.40%	92.32%	78.17%
<i>Salinas</i>	92.63%	95.95%	94.19%

performance of 1.44%, 2.60%, and 3.85% across the three schemes. These differences might be attributed to the level of disparity (domain shift) introduced by the type of patches (uniform only). As 88% of Salinas patches that our single-label classifier originally trained upon were uniform, the domain shift was relatively lower when the classifier was tested on uniform patches. Consequently, the classifier performed better on the new data and across all three schemes. The performance was reduced on the subset of uniform patches dataset taken from PaviaU since the uniform patches generated from this scene accounted for 64% of all patches. In comparison to Salinas, this suggests a more significant domain shift. The observations above are critical if we consider that this uniform-patch setting is the simplest scenario for a single-label prediction classifier. Moreover, it shows that the common practice of assigning the center pixel label to a patch has high costs in performance and is a practice that should be discouraged.

#### 4.5 Multi-label versus Single-label Classifiers: Impact of Extended Annotations on Learning Feature Representation

The goal of this experiment is to determine whether it is possible to improve representation learning by considering richer annotations in the form of multiple labels. In order to answer this question, we compared the performance of the two models, the multi-label and the single-label classifiers. Both models were trained on patch-based datasets, however, one model restricted its predictions to a single label by using more constrained single-label annotations. Towards this goal, we modified our single-label classifier to provide multiple labels as outputs. More specifically, given an input, we selected the class labels corresponding to the top- $k$  logits. Here the number of  $k$  selected logits is equivalent to the number of outputs produced by the multi-label classifier when processing the same input. It is worth indicating that this experiment is conducted using the multi-labeled data defined in Section 3.4 after removing the background class that is one of the classes included in the case of the multi-label classification. This is done to ensure a fair comparison with the results generated from the single-label classification, which ignores the background class.

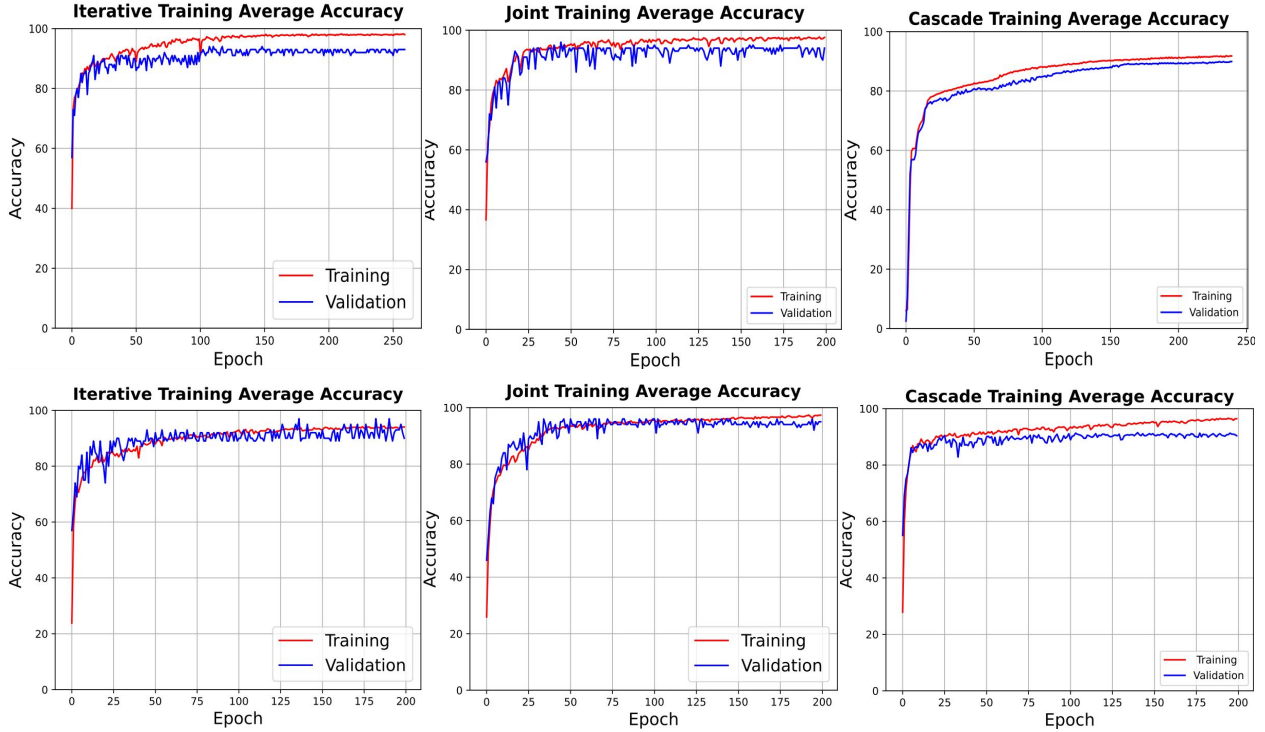

 Figure 6: Single-label Classifier: average accuracy performance - *above*: PaviaU, *below*: Salinas

Table 10 presents the average accuracy that both classifiers achieved across the three schemes; *Iterative*, *Joint* and *Cascade*.

Table 10: Single-label vs Multi-label Classification: performance (in %) on patches with extended annotations

	<i>Iterative</i> classifiers		<i>Joint</i> classifiers		<i>Cascade</i> classifiers	
	<i>multi-label</i>	<i>single-label</i>	<i>multi-label</i>	<i>single-label</i>	<i>multi-label</i>	<i>single-label</i>
<i>PaviaU</i>	90.86	87.07	94.24	95.76	91.10	84.32
<i>Salinas</i>	90.55	90.83	90.49	92.33	89.03	92.60

From the results in Table 10, we can observe that the *Joint* scheme achieved high performance under both classifiers and both datasets. However, the improvement in performance is noticeable when the results of the single-label classifier are compared to those reported under Section 4.3, Table 8. It is evident that the single-label classifier trained using the *Joint* scheme learned a representation sufficiently accurate to achieve better results when we do not limit its prediction to the highest logit generated.

Under the *Cascade* scheme, the behavior of both the multi-label and the single-label classifiers was related to the nature of the data. Considering the multi-label context, the *Cascade* scheme performed better under PaviaU than under Salinas. Most remarkably, the multi-label classifier performance under the *Cascade* scheme was better when ignoring the background class compared to the results presented in Section 4.1, Tables 5 and 6.

When examining the results of the single-label classifier trained using the *Iterative* scheme, we notice that it achieved lower accuracy compared to the results of Section 4.3, Table 8. In other words, when the prediction of the single-label classifier in this context was not limited to the highest logit, it had lower performance. Such result indicates that the classifier trained using the *Iterative* scheme was only successful in learning the representations related to the center pixel of the patch (the one to which the label of the patch corresponds) and failed to learn representations related to the full patch.

#### 4.6 Training Schemes: Accuracy per Class

This experiment highlights how accurate each classifier is in predicting the correct class considering the three training schemes. We base our evaluation on the patches test dataset sampled from both PaviaU and Salinas scenes.

##### 4.6.1 Single-label classifier

Table 11 presents the accuracy of the single-label classifier in predicting the classes of the PaviaU scene. The per-class accuracy results confirm the rankings defined based on the global performance observed in the previous experiments. The *Joint* training scheme detected 77.78% of the classes with an accuracy of 90% and above. The *Iterative* training scheme detected 55.56% of the classes with an accuracy exceeding 90% whereas the *Cascade* training scheme detected 44.45% of the classes with an accuracy exceeding 96%.

Table 11: Single-label Classifier: per-class accuracy measured on PaviaU patches test dataset. *Frequency* stands for the count of the patch instances labeled with the corresponding class.

<i>Class</i>	<i>Frequency</i>	<i>Iterative</i> %	<i>Joint</i> %	<i>Cascade</i> %
1 <i>Asphalt</i>	84	78.63	86.33	80.95
2 <i>Meadows</i>	214	100.00	98.13	96.73
3 <i>Gravel</i>	20	100.00	90.00	60.00
4 <i>Trees</i>	33	95.85	100.00	100.00
5 <i>Metal Sheet</i>	18	93.72	100.00	100.00
6 <i>Soil</i>	46	90.60	100.00	76.09
7 <i>Bitumen</i>	13	87.63	84.62	53.85
8 <i>Brick</i>	43	83.23	90.70	88.37
9 <i>Shadows</i>	13	74.47	100.00	100.00

Table 12: Single-label Classifier: per-class accuracy measured on Salinas patches test dataset. *Frequency* stands for the count of the patch instances labeled with the corresponding class.

<i>Class Name</i>	<i>Frequency</i>	<i>Iterative</i> %	<i>Joint</i> %	<i>Cascade</i> %
1 <i>Brocoli_1</i>	25	78.63	86.33	80.95
2 <i>Brocoli_2</i>	49	100.00	100.00	100.00
3 <i>Fallow</i>	25	96.00	100.00	96.00
4 <i>Fallow_r</i>	17	100.00	100.00	100.00
5 <i>Fallow_s</i>	24	100.00	100.00	100.00
6 <i>Stubble</i>	45	100.00	100.00	100.00
7 <i>Celeray</i>	41	100.00	100.00	100.00
8 <i>Grapes</i>	119	73.95	91.60	71.43
9 <i>Soil</i>	67	100.00	100.00	100.00
10 <i>Corn</i>	34	85.29	88.24	85.29
11 <i>Lettuce_4</i>	11	81.82	81.82	81.82
12 <i>Lettuce_5</i>	15	100.00	100.00	100.00
13 <i>Lettuce_6</i>	10	90.00	100.00	100.00
14 <i>Lettuce_7</i>	8	100.00	100.00	87.50
15 <i>Vinyard</i>	88	85.23	72.73	81.82
16 <i>Vinyard-Vert</i>	24	100.00	100.00	100.00

Furthermore, Table 12 displays the performance of the single-label classifier on the Salinas dataset and across three schemes. The classifier equally predicted 100% of the correct instances of 9 out of the 16 classes available in the Salinas dataset. The *Joint* scheme eventually outperformed both the *Iterative* and the *Cascade* schemes in predicting 4 out of the remaining 8 classes positioning it at the highest rank in terms of accuracy-per-class performance among the three schemes.

##### 4.6.2 Multi-label classifier

Table 13 summarizes the performance of the multi-label classifier tested on the multi-label patches test dataset sampled from PaviaU. Based on the results, the three schemes led to models with similar predictive performance. In

predicting the background class, both the *Joint* and *Cascade* schemes performed slightly lower compared to the *Iterative* variant. However, the performance of the three schemes on this class was lower compared to their performance on the remaining classes. Approximately 20% of the Background labels were incorrectly predicted by the classifier. This explains why in Section 4.5 we noticed the improvement in the overall performance of the multi-label classifier when we ignored the Background class. Table 14, presents the per-class performance for each scheme on the Salinas multi-label patches test dataset. Apart from the results on the *Background* class, the three schemes have relatively close and high accuracy rates.

Table 13: Multi-label Classifier: per-class accuracy measured on PaviaU patches test dataset. *Frequency* corresponds to how many times the class appeared in the multi-labels assigned to the patches. It does not resemble the count of the patches whose labels correspond to a particular class.

<i>Class</i>	<i>Name</i>	<i>Frequency</i>	<i>Iterative</i>	<i>Joint</i>	<i>Cascade</i>
0	<b>Background</b>	400	81.45	78.99	79.13
1	<b>Asphalt</b>	118	97.54	97.68	97.54
2	<b>Meadows</b>	237	95.51	98.55	96.52
3	<b>Gravel</b>	47	97.83	97.39	97.83
4	<b>Trees</b>	88	98.70	98.84	98.70
5	<b>Metal Sheet</b>	19	100.00	100.00	100.00
6	<b>Soil</b>	50	96.52	99.71	97.54
7	<b>Bitumen</b>	20	98.41	98.99	98.84
8	<b>Brick</b>	85	97.54	97.10	97.10
9	<b>Shadows</b>	26	99.86	100.00	100.00

Table 14: Multi-label Classifier: per class accuracy measured on Salinas patches test dataset. *Frequency* corresponds to how many times the class appeared in the multi-labels assigned to the patches. It does not resemble the count of the patches whose labels correspond to a particular class.

<i>Class</i>	<i>Name</i>	<i>Frequency</i>	<i>Iterative</i>	<i>Joint</i>	<i>Cascade</i>
0	<b>Background</b>	148	87.39	87.39	85.02
1	<b>Brocoli_1</b>	26	100.00	99.85	100.00
2	<b>Brocoli_2</b>	49	100.00	100.00	100.00
3	<b>Fallow</b>	22	99.70	99.85	100.00
4	<b>Fallow_r</b>	20	99.85	99.70	99.70
5	<b>Fallow_s</b>	37	99.56	99.56	99.70
6	<b>Stubble</b>	48	99.85	99.85	99.85
7	<b>Celeray</b>	35	99.70	99.56	99.85
8	<b>Grapes</b>	140	93.77	93.77	92.58
9	<b>Soil</b>	82	99.70	99.70	99.41
10	<b>Corn</b>	42	98.22	98.81	98.67
11	<b>Lettuce_4</b>	18	99.70	100.00	99.26
12	<b>Lettuce_5</b>	22	99.70	99.41	99.41
13	<b>Lettuce_6</b>	15	99.85	99.85	99.85
14	<b>Lettuce_7</b>	19	99.56	99.56	99.70
15	<b>Vinyard</b>	83	93.92	94.21	93.03
16	<b>Vinyard-Vert</b>	16	99.85	100.00	100.00

## 4.7 Comparison With Existing Work

In this section, we quantitatively compare the performance obtained in our study with two related methods from the literature. This is done on two fronts. First, at the data level, we trained and tested the HSI-CNN method developed in [34] using the single label patches dataset we sampled. Second, at the training scheme level, we trained in a joint manner and tested the two branch autoencoder method (TBAE) developed in [21] using the patches dataset and compared the performance with that of our two-component network, (Section 3).

### 4.7.1 Single-label Classifier Performance: Training Different Architectures using Patches Dataset

The experiment investigates whether the performance of the single-label classifier trained with a smaller number of patches would differ given the different underlying architecture employed for learning representations.



In [34], the classification method is based on a convolutional neural network to perform the hyperspectral image classification task whereas our network adopts an architecture of fully connected layers. Similar to our work, the HSI-CNN method is trained using patches of  $n \times n \times \text{bands}$  extracted from the original remote sensing scene to preserve the spatial-spectral aspect of the data. In addition, assigning labels to patches is based on the label corresponding to the center pixel, a protocol we also use for our single labeled patches. There is, however, one point to note. The sampling process originally followed in [34] differs from ours. They perform a dense sampling that maintains the same count of labels of the original remote sensing scene, whereas in sampling our patches we ensured that no overlapping between the patches is allowed. This reduces the volume of the dataset and the count of the labels. By doing so we reduce the computational time and the required resources to conduct the experiments.

Table 15: Single label Classification: accuracy performance (in%) of the two-component network under the three training schemes, the HSI-CNN method trained using the *non-overlapping* patches dataset, the HSI-CNN method trained using *densely* sampled patches and the TBAE method trained using the *non-overlapping* patches dataset

	<i>Iterative</i>	<i>Joint</i>	<i>Cascade</i>	<i>HSI-CNN</i> <i>non-overlapping</i>	<i>HSI-CNN</i> <i>dense</i>	<i>TBAE</i>
<i>Pavia</i>	90.71	94.65	87.73	70.56	73.05	89.56
<i>Salinas</i>	91.19	93.35	90.34	87.33	69.05	91.96

We based our experiment on the implementation of the HSI-CNN method provided by [11] in their DeepHyperX toolbox [38]. Given that the volume of the input data and the process of sampling are different, training the model required tuning a set of hyperparameters that is not completely identical. Similar to the DeepHyperX implementation, we used the stochastic gradient descent (SGD) optimizer, a cross-entropy loss function and a learning rate scheduler. Moreover, opposite to the mentioned implementation the scheduler differed from one dataset to the other. For the PaviaU dataset, we used the step-learning rate scheduler which enforces a reduction in the learning rate value at the end of a predefined set of epochs. This learning rate adaptation, however, did not work for Salinas dataset, where we applied the reduce-on-plateau scheduler. When the model was trained on patches extracted from the Salinas dataset, empirical evidence suggested that the learning rate reduction pattern was not correctly captured using a predefined number of epochs. In contrast, the reduced on plateau scheduler allowed the model to automatically adjust the learning rate when the validation loss performance stopped improving rather than enforcing a fixed period to apply the change. All details related to the hyperparameters can be found in the supplementary material.

Table 15 contrasts the results of training the CNN-HSI method using the non-overlapping patches dataset sampled in our work against the results achieved by the DeepHyperX implementation of the the same method using the densely sampling process of patches proposed by [34].

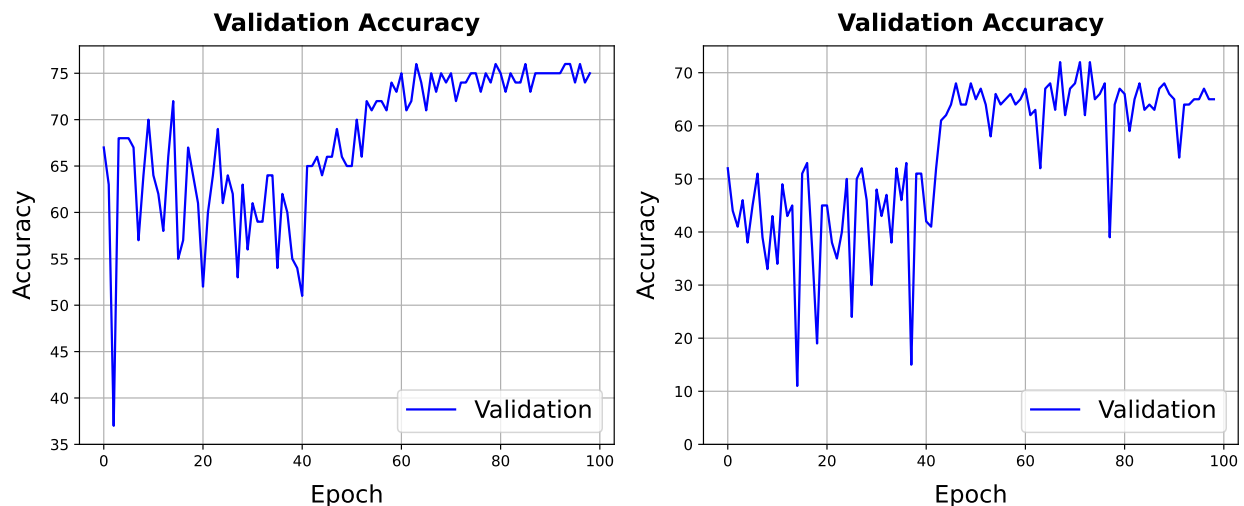


Figure 7: Validation accuracy performance of the HSI-CNN method developed by [34] and implemented by [11] using *densely* sampled patches from the remote sensing scenes. *Left: PaviaU, right: Salinas*

Figures 7 and 8 contrast the performance of the DeepHyperX implementation against our implementation of the HSI-CNN method using the dataset of patches that we originally used to train our own two-component network. Both



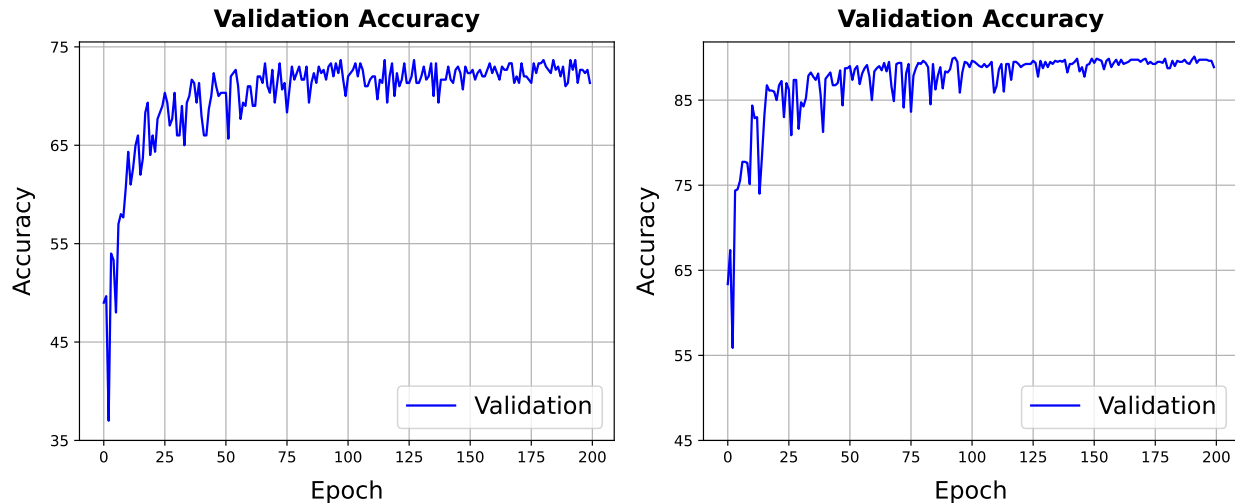


Figure 8: Validation accuracy performance of the method developed by [34] and implemented by [11] that we amended to use our sampled *non-overlapping* patches dataset. *Left: PaviaU, right: Salinas*

our results and those achieved by the DeepHyperX implementation could not match those reported in [34]. This is not surprising, given the fact that we are using a different dataset and a different set of hyperparameters. Nevertheless, we did observe one similar behavior in our implementation of the results reported in the original paper: the progressive upward sloping of the accuracy curves.

In summary, the high correlation between a pixel and its neighboring pixels, which share common characteristics, can be captured when a model is trained using patches datasets, as opposed to spectral-only pixels. The nature of patches can provide an option to overcome the shortcoming of having limited labeled datasets. Hence, in the absence of large labeled samples of remote sensing datasets, deep architectures like the one presented in [34] can be easily and more efficiently trained on a smaller-sized dataset. One that preserves both the spatial and the spectral dimensions and leverages the correlation between the neighboring pixels.

#### 4.7.2 Single-label Classifier Performance: *Joint* Training Scheme

[21] presents a semi-supervised method that extracts features from the unlabeled data by training a single-layer autoencoder whose hidden layer inputs into a classifier with a Softmax layer. Simultaneously, the encoder and the classifier exploit the labeled data to perform a classification task. In their analysis they show the possibility of jointly training the two-branch autoencoder (TBAE) model using a limited number of unlabeled and labeled pixels of the remote sensing scenes. Their work appears to share structural similarity with our work in terms of the two-component architecture encompassing an autoencoder and a classifier and combined with the *Joint* training scheme. Based on that, we reproduced their method and allowed the training to proceed using our single-label patches dataset, sampled from PaviaU and Salinas in accordance to the *Single-label sampling* approach described in Section 3.4.

Figure 9 exhibits the results of the training conducted. Even with the shallowness of the architecture, the joint training of the model allowed good performance in terms of validation accuracy. The latter achieved on average 89.56% on the PaviaU patches dataset and 91.96% on the Salinas patches dataset, (Table 15). However, this performance fell short when compared with the results achieved by our architecture (Section 3) trained using the *Joint* scheme which was 94.65% and 93.35% on PaviaU and Salinas, respectively (Section 4.3, Table 8). In our opinion, this is justified for two main reasons. First, the deeper architecture of our two-component network, which allows the encoding of a richer representation. Second, the different shape of the input data, i.e., the patches, which preserves the joint spatial-spectral aspect of the original remote sensing scene. As opposed to the method from [21], which was trained using pixels containing only spectral information. Furthermore, the results demonstrate that our architecture is capable of learning intrinsic feature representations embedded in the patches despite their limited volume.

## 5 Conclusion

In this paper, we trained a two-component network of an autoencoder and a classifier to perform a multi-label hyperspectral classification task. We shifted away from the single-label pixel-level input data. Instead we focused on

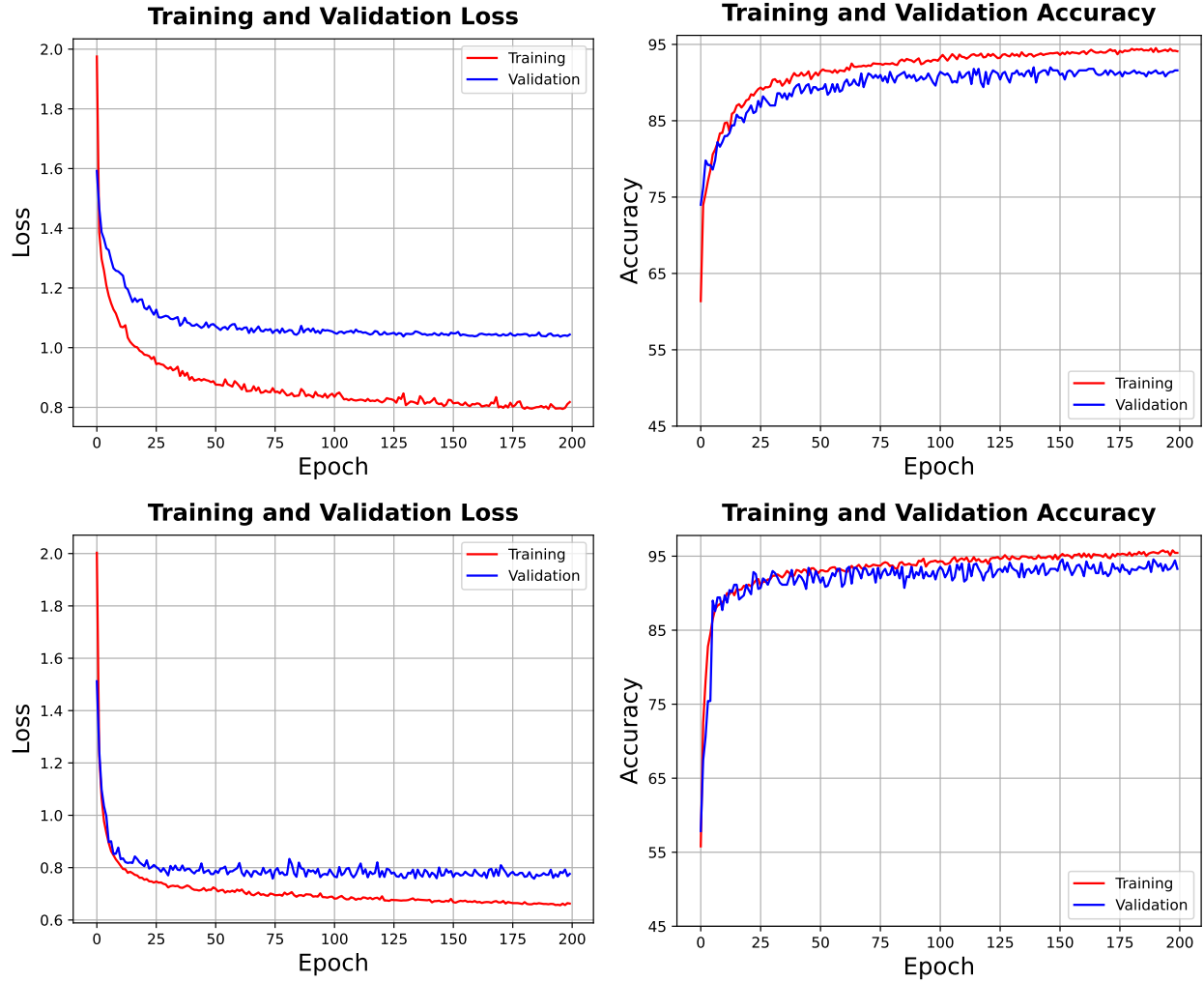


Figure 9: Performance in terms of loss and accuracy on the method developed by [21] using *non-overlapping* sampled patches. *Above*: PaviaU, *below*: Salinas

patches extracted from the the hyperspectral remote sensing scenes to leverage the abundance of information available in those scenes and the correlation among the pixels. We trained our network and compared the performance of the trained classifier when those patches were assigned multi-labels instead of single labels. In addition to the *Joint* and *Cascade* training schemes of the two-component network frequently utilized in the literature, we investigated the *Iterative* training scheme. Under two datasets and two different classification tasks, multi-label and multi-class classification, we found that the *Cascade* scheme performs the least. the *Joint* scheme performed the highest under all scenarios. However, it suffers the drawback of requiring an expensive parameter search procedure to find the best weight combination of the total loss constituents and this may come at the risk of overfitting. Such a combination could be optimal given a specific data split and selected hyperparameters; however, there is no guarantee that this combination could generalize given other conditions and hyperparameters. According to our experiments, the *Iterative* scheme with its progressive learning allows the sharing of features between the two parts of the network from the early stages of training. Its application does not require any search process for specific hyperparameters that is not evident or principled and produces good results. This is noticeable with complex datasets containing many multi-label patches that preserve hyperspectral images' spatial and spectral properties. Further, experiments suggest that the common practice of assigning a label corresponding to the center pixel of a patch has high costs in predictive performance. This is a practice that should be discouraged. Furthermore, we show that deeper architectures with a completely different nature than our two-component network could perform well when trained on datasets smaller in volume yet more abundant in spatial-spectral information. By this, we mean the patches dataset used in our experiments. We also found that when using the Joint scheme to train our two-component architecture with patches, the performance was much higher than training a shallower architecture with a small subset of labeled pixels containing only spectral information. As

future work, our study can be extended by further validating the covered schemes and methods on other remote sensing datasets and possibly other types of hyperspectral images. Recent learning techniques; such as self-supervised learning, and modern architectures; such as transformers, will be considered to further boost the performance of our classifier.

## Acknowledgments

The research presented in this article is part of the project "Learning-based representations for the automation of hyperspectral microscopic imaging and predictive maintenance" funded by the Flanders Innovation & Entrepreneurship - VLAIO, under grant number HBC.2020.2266.

## References

- [1] Alexander F.H. Goetz. Three decades of hyperspectral remote sensing of the earth: A personal view. *Remote Sensing of Environment*, 113:S5–S16, 2009.
- [2] Muhammad Jaleed Khan, Hamid Saeed Khan, Adeel Yousaf, Khurram Khurshid, and Asad Abbas. Modern trends in hyperspectral image analysis: A review. *Ieee Access*, 6:14118–14129, 2018.
- [3] Prem Chandra Pandey, Heiko Balzter, Prashant K. Srivastava, George P. Petropoulos, and Bimal Bhattacharya. Future perspectives and challenges in hyperspectral remote sensing. In *Hyperspectral Remote Sensing*, pages 429–439. Elsevier, 2020.
- [4] Tammy Jiang, Jaimie L. Gradus, and Anthony J. Rosellini. Supervised machine learning: A brief primer. *Behavior Therapy*, 51(5):675–687, 2020.
- [5] He Sun, Lei Zhang, Jinchang Ren, and Hua Huang. Novel hyperbolic clustering-based band hierarchy (hcbh) for effective unsupervised band selection of hyperspectral images. *Pattern Recognition*, 130:108788, 2022.
- [6] Shrutika Sawant and Manoharan Prabukumar. A survey of band selection techniques for hyperspectral image classification. *Journal of Spectral Imaging*, 9(1):a5, 2020.
- [7] Behnood Rasti, Danfeng Hong, Renlong Hang, Pedram Ghamisi, Xudong Kang, Jocelyn Chanussot, and Jon Atli Benediktsson. Feature extraction for hyperspectral imagery: The evolution from shallow to deep: Overview and toolbox. *IEEE Geoscience and Remote Sensing Magazine*, 8(4):60–88, 2020.
- [8] Dalal AL-Alimi, Mohammed A.A. Al-qaness, Zhihua Cai, and Eman Ahmed Alawamy. Ida: Improving distribution analysis for reducing data complexity and dimensionality in hyperspectral images. *Pattern Recognition*, 134:109096, 2023.
- [9] Hao Wu and Saurabh Prasad. Semi-supervised dimensionality reduction of hyperspectral imagery using pseudo-labels. *Pattern Recognition*, 74:212–224, 2018.
- [10] Quanhua Zhao, Shuhan Jia, and Yu Li. Hyperspectral remote sensing image classification based on tighter random projection with minimal intra-class variance algorithm. *Pattern Recognition*, 111:107635, 2021.
- [11] Nicolas Audebert, Bertrand Le Saux, and Sebastien Lefevre. Deep learning for classification of hyperspectral data: A comparative review. *IEEE geoscience and remote sensing magazine*, 7(2):159–173, 2019.
- [12] Xiaofei Yang, Yunming Ye, Xutao Li, Raymond Lau, Xiaofeng Zhang, and Xiaohui Huang. Hyperspectral image classification with deep learning models. *IEEE Transactions on Geoscience and Remote Sensing*, PP:1–16, 2018.
- [13] Mengxin Han, Runmin Cong, Xinyu Li, Huazhu Fu, and Jianjun Lei. Joint spatial-spectral hyperspectral image classification based on convolutional neural network. Image/Video Understanding and Analysis (IUVA). *Pattern Recognition Letters*, 130:38–45, 2020.
- [14] Yunsong Li, Weiyang Xie, and Huaqing Li. Hyperspectral image reconstruction by deep convolutional neural network for classification. *Pattern Recognition*, 63:371–383, 2017.
- [15] Jie Zhou, Ganqu Cui, Shengding Hu, Zhengyan Zhang, Cheng Yang, Zhiyuan Liu, Lifeng Wang, Changcheng Li, and Maosong Sun. Graph neural networks: A review of methods and applications. *AI Open*, 1:57–81, 2020.
- [16] Sheng Wan, Shirui Pan, Shengwei Zhong, Jie Yang, Jian Yang, Yibing Zhan, and Chen Gong. Multi-level graph learning network for hyperspectral image classification. *Pattern Recognition*, 129:108705, 2022.
- [17] N. Keshava and J.F. Mustard. Spectral unmixing. *IEEE Signal Processing Magazine*, 19(1):44–57, 2002.
- [18] Amol D. Vibhute, Sandeep V. Gaikwad, Karbhari V. Kale, and Arjun V. Mane. Hyperspectral image unmixing for land cover classification. In *2021 IEEE India Council International Subsections Conference (INDISCON)*, pages 1–5, 2021.

- [19] Alan J.X. Guo and Fei Zhu. Improving deep hyperspectral image classification performance with spectral unmixing. *Signal Processing*, 183:107949, 2021.
- [20] Qiongying Fu, Xuchu Yu, Xiangpo Wei, and Zhixiang Xue. Semi-supervised classification of hyperspectral imagery based on stacked autoencoders. In *Eighth International Conference on Digital Image Processing (ICDIP 2016)*, volume 10033, page 100332B. International Society for Optics and Photonics, 2016.
- [21] Z Lei, Z Yi, L Peng, and SX Hui. Semi-supervised classification of hyperspectral images based on two branch autoencoder. In *IOP Conference Series: Earth and Environmental Science*, volume 502, page 012014. IOP Publishing, 2020.
- [22] Muhammad Ahmad, Sidrah Shabbir, Swalpa Kumar Roy, Danfeng Hong, Xin Wu, Jing Yao, Adil Mehmood Khan, Manuel Mazzara, Salvatore Distefano, and Jocelyn Chanussot. Hyperspectral image classification—traditional to deep models: A survey for future prospects. *IEEE Journal of Selected Topics in Applied Earth Observations and Remote Sensing*, 15:968–999, 2022.
- [23] M.E. Paoletti, J.M. Haut, J. Plaza, and A. Plaza. Deep learning classifiers for hyperspectral imaging: A review. *ISPRS Journal of Photogrammetry and Remote Sensing*, 158:279–317, 2019.
- [24] Qiangqiang Yuan, Huanfeng Shen, Tongwen Li, Zhiwei Li, Shuwen Li, Yun Jiang, Hongzhang Xu, Weiwei Tan, Qianqian Yang, Jiwen Wang, Jianhao Gao, and Liangpei Zhang. Deep learning in environmental remote sensing: Achievements and challenges. *Remote Sensing of Environment*, 241:111716, 2020.
- [25] Onuwa Okwuashi and Christopher E. Ndehedehe. Deep support vector machine for hyperspectral image classification. *Pattern Recognition*, 103:107298, 2020.
- [26] Cong Wang, Peng Zhang, Yanning Zhang, Lei Zhang, and Wei Wei. A multi-label hyperspectral image classification method with deep learning features. In *Proceedings of the International Conference on Internet Multimedia Computing and Service*, pages 127–131, 2016.
- [27] Jing Zhang, PeiXian Ding, and Shuai Fang. Multi-label classification of hyperspectral images based on label-specific feature fusion. In *Neural Information Processing*, pages 224–234. Springer International Publishing, 2021.
- [28] Radamanthys Stivaktakis, Grigorios Tsagkatakis, and Panagiotis Tsakalides. Deep learning for multilabel land cover scene categorization using data augmentation. *IEEE Geoscience and Remote Sensing Letters*, 16(7):1031–1035, 2019.
- [29] Madhumitha Ramamurthy, Y. Harold Robinson, S. Vimal, and A. Suresh. Auto encoder based dimensionality reduction and classification using convolutional neural networks for hyperspectral images. *Microprocessors and Microsystems*, 79:103280, 2020.
- [30] Swati Priya, Ranendu Ghosh, and BK Bhattacharya. Non-linear autoencoder based algorithm for dimensionality reduction of airborne hyperspectral data. *The International Archives of Photogrammetry, Remote Sensing and Spatial Information Sciences*, 42:593–598, 2019.
- [31] Xing Chen, Li Ma, and Xiaoquan Yang. Stacked denoise autoencoder based feature extraction and classification for hyperspectral images. *J. Sensors*, 2016:3632943:1–3632943:10, 2016.
- [32] Elham Kordi Ghasrodashti and Nabin Sharma. Hyperspectral image classification using an extended auto-encoder method. *Signal Processing: Image Communication*, 92:116111, 2021.
- [33] Akrem Sellami and Salvatore Tabbone. Deep neural networks-based relevant latent representation learning for hyperspectral image classification. *Pattern Recognition*, 121:108224, 2022.
- [34] Yanan Luo, Jie Zou, Chengfei Yao, Xiaosong Zhao, Tao Li, and Gang Bai. Hsi-cnn: a novel convolution neural network for hyperspectral image. In *2018 International Conference on Audio, Language and Image Processing (ICALIP)*, pages 464–469, 2018.
- [35] Diederik Kingma and Jimmy Ba. Adam: A method for stochastic optimization. *International Conference on Learning Representations*, 2014.
- [36] Hyperspectral remote sensing scenes. Accessed: 23-12-2022. [https://www.ehu.eus/ccwintco/index.php/Hyperspectral\\_Remote\\_Sensing\\_Scenes](https://www.ehu.eus/ccwintco/index.php/Hyperspectral_Remote_Sensing_Scenes), 2011.
- [37] Mohammad S Sorower. A literature survey on algorithms for multi-label learning. *Oregon State University, Corvallis*, 18:1–25, 2010.
- [38] Deephyperx: Deep learning toolbox based on pytorch for hyperspectral data classification. "<https://github.com/nshaud/DeepHyperX>", 2020. Accessed: 23-12-2022.

## 6 Supplementary Material

### 6.1 Introduction

In this document, we introduce additional details and information about the work we conducted to facilitate the replication of the two-component network we designed and the training schemes we explored. In Section 6.2 we introduce all hyperparameters tuned for each scheme under the multi-label as well as the single-label classification task. In Section 6.3 we add the relevant hyperparameters we used to train the two methods from the literature that we reproduced and trained using the patches datasets we sampled.

### 6.2 Hyperparameters for each training scheme

In this section, we present the relevant hyperparameters selected for training the network under each scheme we proposed. We selected the hyperparameters that generated the highest performance across the three schemes. Sections 6.2.1 and 6.2.2 relate to experiments under Sections 4.1 and 4.3 of the original paper, respectively. In them, We provide information that will allow reproducing the results achieved under the mentioned sections. Furthermore, under section 6.2.3 we provide the mathematical representation of the evaluation metrics used in the multi-label classification context.

#### 6.2.1 Multi-Label Classification: Performance Across Training Schemes

In this experiment we trained the multi-label classifier under the three training schemes, *Iterative*, *Joint*, *Cascade*, using multi-labeled patches. We sampled those patches under the *multi-label sampling* approach as defined under Section (3.4) in the original paper. Table 16 presents the hyperparameters used for performing the experiment in Section 4.1. Those hyperparameters were used to train the two-component network for multi-label classification task following the three schemes, on patches sampled from PaviaU dataset. Table 17 presents the hyperparameters used for performing the experiment in Section (4.1) to train the two-component network for multi-label classification task under the three schemes, however using patches sampled from Salinas dataset.

Table 16: Multi-label classification: Hyperparameters adopted for the three training schemes using multi-labeled patches sampled from PaviaU dataset.

<i>Parameter</i>	<i>Iterative</i>	<i>Joint</i>	<i>Cascadet</i>
<i>Batch size</i>	200	200	200
<i>Epochs-AE</i>	95	95	95
<i>Epochs-Clf</i>	200	200	200
<i>Iterative Epochs</i>	20	—	—
<i>Lr-AE</i>	$1e^{-2}$	$1e^{-2}$	$1e^{-2}$
<i>Lr-Clf</i>	$1e^{-2}$	$1e^{-2}$	$1e^{-2}$
<i>Lr-step_size AE</i>	10	15	15
<i>Lr-step_size Clf</i>	15	15	15
<i>Lr-scheduler<math>\gamma</math></i>	0.9	0.9	0.9
<i>dropout _AE</i>	0.3	.3	0.3
<i>dropout _Clf</i>	0.6	0.6	0.6
<i>L2-Regularization</i>	0.0001	0.0001	0.0001

#### 6.2.2 Single-Label Classification: Performance Across Training Schemes

Under this experiment, we trained the two-component network for the single-label classification task. For that purpose, we utilized single labeled patches sampled under the *Single label sampling* approach. Tables 18 and 19 provide a summary of the hyperparameters tuned for the highest performance for each of the three training schemes, *Iterative*, *Joint*, *Cascade*.

#### 6.2.3 Multi-label Classification: Evaluation Metrics.

The equations below define the evaluation metrics we calculated to evaluate the performance of the three training schemes, *Iterative*, *Joint*, *Cascade* within the multi-label classification task. For that we adopted the measures used in [37].

Table 17: Multi-label classification: Hyperparameters adopted for the three training schemes using multi-labeled patches sampled from Salinas dataset.

<i>Parameter</i>	<i>Iterative</i>	<i>Joint</i>	<i>Cascade</i>
<i>Batch size</i>	130	130	130
<i>Epochs-AE</i>	95	95	95
<i>Epochs-Clf</i>	200	200	240
<i>Iterative Epochs</i>	20	—	—
<i>Lr-AE</i>	$1e^{-2}$	$1e^{-2}$	$1e^{-2}$
<i>Lr-Clf</i>	$1e^{-2}$	$1e^{-3}$	$1e^{-5}$
<i>Lr-step_size AE</i>	10	20	15
<i>Lr-step_size Clf</i>	15	20	15
<i>Lr-scheduler <math>\gamma</math></i>	0.9	0.9	0.9
<i>Dropout_Clf</i>	0.6	0.6	0.6
<i>L2 -Regularization</i>	0.0001	0.0001	0.0001

Table 18: Single-label classification: Hyperparameters adopted for each training scheme using patches sampled from PaviaU dataset.

<i>Parameter</i>	<i>Iterative</i>	<i>Joint</i>	<i>Cascade</i>
<i>Batch size</i>	240	164	100
<i>Epochs-AE</i>	95	95	95
<i>Epochs-Clf</i>	260	200	240
<i>Iterative Epochs</i>	20	—	—
<i>Lr-AE</i>	$1e^{-2}$	$1e^{-2}$	$1e^{-2}$
<i>Lr-Clf</i>	$1e^{-3}$	$1e^{-3}$	$1e^{-5}$
<i>Lr-step_size AE</i>	10	20	15
<i>Lr-step_size Clf</i>	10	20	15
<i>Lr-scheduler <math>\gamma</math></i>	0.9	0.9	0.9
<i>Dropout_Clf</i>	0.6	0.6	0.6
<i>L2 -Regularization</i>	0.0009	0.001	0.0001

Table 19: Single-label classification: Hyperparameters adopted for each training scheme using patches sampled from Salinas dataset.

<i>Parameter</i>	<i>Iterative</i>	<i>Joint</i>	<i>Cascade</i>
<i>Batch size</i>	240	200	200
<i>Epochs-AE</i>	95	95	95
<i>Epochs-Clf</i>	200	200	200
<i>Iterative Epochs</i>	20	—	—
<i>Lr-AE</i>	$1e^{-3}$	$1e^{-3}$	$1e^{-3}$
<i>Lr-Clf</i>	$1e^{-3}$	$1e^{-3}$	$1e^{-3}$
<i>Lr-step_size AE</i>	10	10	10
<i>Lr-step_size Clf</i>	10	10	10
<i>Lr-scheduler <math>\gamma</math></i>	0.9	0.9	0.9
<i>Dropout_Classifier</i>	0.6	0.6	0.6
<i>L2 -Regularization</i>	0.0009	0.0007	0.0009

$$Hamming - Loss = \frac{1}{n, L} \sum_{i=1}^n \sum_{j=1}^L I(y_i^j \neq \hat{y}_i^j)$$

$$Accuracy = \frac{1}{n} \sum_{i=1}^n \frac{|y_i \cap \hat{y}_i|}{|y_i \cup \hat{y}_i|}$$

$$Precision = \frac{1}{n} \sum_{i=1}^n \frac{|y_i \cap \hat{y}_i|}{|\hat{y}_i|}$$

$$Recall = \frac{1}{n} \sum_{i=1}^n \frac{|y_i \cap \hat{y}_i|}{|y_i|}$$

### 6.3 Comparison with existing work

We selected two relevant methods in the literature with the purpose of evaluating their performance, on the patches dataset we generated. Hence, we reproduced the same architecture of the two methods however, the training process takes into consideration the shape of our patches dataset. Since the new data differs from the original one used to train those methods, we had to tune the hyperparameters to achieve a good results on our dataset.

#### 6.3.1 Patches dataset or densely sampled pixels with neighbourhood

In the section we present the hyperparameters we used to train the method reproduced from [34]. As mentioned in the original paper, we reproduced the same architecture, however, due to lack of complete details of implementation we fine-tuned our own hyperparameters to train this network using our patches datasets from PaviaU and Salinas. Table 20 presents the details.

Table 20: Hyperparameters for training the method developed by [34]

<i>Parameter</i>	<i>PaviaU</i>	<i>Salinas</i>
<i>Batch size</i>	100	164
<i>Epochs</i>	200	200
<i>Lr</i>	$1e^{-3}$	$1e^{-3}$
<i>Lr-Scheduler</i>	StepLR	ReduceLROnPlateau
<i>Lr-step/patience</i>	20	5
$\gamma$ /factor	0.9	0.9
<i>Weight_decay</i>	0.09	0.09

#### 6.3.2 Joint training using small sized dataset

In the section we present the hyperparameters we used to train the method reproduced from [21]. The purpose was to reproduce their architecture and train it using the patches datasets we sampled. Although in their paper they do not test their method using Salinas datasets, however, we chose to perform an experiment using patches sampled from Salinas dataset since aim is to test the performance of such method on the data that we sampled and used to train our two-component network.

Table 21: Hyperparameters for training the method developed by [21]

<i>Parameter</i>	<i>PaviaU</i>	
<i>Batch size</i>	100	100
<i>Epochs</i>	200	200
<i>Lr</i>	$1e^{-2}$	$1e^{-2}$
<i>Lr-step</i>	10	20
$\gamma$	0.9	0.9
<i>L2-Regularization</i>	0.0001	0.0001